Low-frequency excitation of length of day and polar motion by the atmosphere

Olivier de Viron,[1] David Salstein,[2] Christian Bizouard,[3] and Laura Fernandez[4]

Received 30 September 2003; revised 9 January 2004; accepted 16 January 2004; published 19 March 2004.

[1] Results of a 100-year run of the Hadley Centre general circulation model are used to compute monthly values of the three components of atmospheric torque on the Earth and of the associated atmospheric angular momentum series. All these results are compared with equivalent ones from the National Center for Environmental Prediction/National Center for Atmospheric Research reanalyses for the overlap period since 1948. We find some important differences; consequently, our results should be taken as an order of magnitude of the effect. We also compute the effect of the atmosphere on length of day (LOD) and polar motion by the use of both the torque and the angular momentum approaches. We find comparable amplitude with both torque and angular momentum for the polar motion; the axial torque, however, related to LOD, appears to be unphysical. The excitation of long-period LOD variation is in phase with the observed variation but much smaller. The low-frequency polar motion is only coherent with the observation at certain particular periods. *INDEX TERMS:* 1223 Geodesy and Gravity: Ocean/Earth/atmosphere interactions (3339); 1239 Geodesy and Gravity: Rotational variations; 3339 Meteorology and Atmospheric Dynamics: Ocean/atmosphere interactions (0312, 4504); *KEYWORDS:* Earth rotation, atmosphere-Earth interaction

Citation: de Viron, O., D. Salstein, C. Bizouard, and L. Fernandez (2004), Low-frequency excitation of length of day and polar motion by the atmosphere, *J. Geophys. Res.*, *109*, B03408, doi:10.1029/2003JB002817.

1. Introduction

[2] The rotation of the Earth is not constant with time: the rotation rate shows fluctuations over a broad range of frequencies, causing variation of the length of day (LOD) and of the direction of the rotation axis, whose motions are both in the inertial frame (precession and nutation) and within the Earth's figure (polar motion).

[3] LOD fluctuations at interannual to subdiurnal frequencies are mainly due to the interaction between the Earth and its atmosphere. The oceans and other aspects of hydrology contribute to a much lesser extent [see *Marcus et al.*, 1998; *Chen et al.*, 2000]. At the decadal timescale, additionally, interactions between the Earth's core and overlying mantle are considered to be the major cause of LOD fluctuation; a high correlation between the LOD and the first harmonics of the magnetic field time series exists at those timescale [*Ball et al.*, 1969]. The effects of the atmosphere and ocean on the decadal fluctuations of the LOD are small, though they may be related to cycles of total solar irradiance [*Abarca del Rio et al.*, 2000]. Overall, polar motion on the broad range of interannual to subdiurnal frequencies may be attributed to the effect of the oceans (about 60%, depending on the frequency) and of the atmosphere (about 40%), as shown, for example, by *Ponte et al.* [1998].

[4] At the decadal frequency the Markowitz mode (very elliptical polar motion at long period, more than 25 years, of about 35 milliarc seconds (mas)) is observed in polar motion. At the present time, its causes are not identified. Though it might be expected that the core-mantle interaction could excite decadal polar motion, at present stage, this effect cannot be properly determined.

[5] The evaluation of the overall atmospheric effect depends on the availability and the quality of atmospheric analysis. In the era prior to the direct availability of atmospheric observations to assimilate into such analyzes, global circulation models (GCMs) have been used to simulate the atmosphere on the basis of boundary information from the underlying surface of the atmosphere. Here we use a set of results from a lengthy run covering the twentieth century using the global circulation model from the Hadley Centre, which is forced by global ice conditions and sea surface temperature to evaluate the effect of the atmosphere. Estimations of oceanic excitations, similarly, depend on analyzes and models, though there is very little in situ observations to drive an analysis system.

[6] Classically, two different approaches are used to evaluate the effect of a fluid layer on Earth rotation. In the first approach, the so-called "angular momentum approach," the solid Earth plus fluid layer system is consid-

[1]Royal Observatory of Belgium, Brussels, Belgium.
[2]Atmospheric and Environmental Research, Inc., Lexington, Massachusetts, USA.
[3]Observatoire de Paris, Systèmes of Référence Temps Espace, Paris, France.
[4]Consejo de Investigaciones Cientficas y Técnicas, Facultad de Ciencias Astronomicas y Geofisicas, Buenos Aires, Argentina.

0148-0227/04/2003JB002817$09.00

ered as isolated. Consequently, the angular momentum of the system is conserved, and we have

$$\frac{d\mathbf{H}_{\text{solid Earth}}}{dt} = -\frac{d\mathbf{H}_{\text{fluid layer}}}{dt}, \tag{1}$$

where $\mathbf{H}$ is the angular momentum vector. The angular momentum of the fluid layer is computed from the motion (wind and current) and mass (pressure and density) fields of the fluid, from which the Earth rotation parameters are directly inferred [e.g., *Munk and McDonald*, 1960]. The angular momentum of the fluid layer is classically decomposed into two parts, the matter and the motion term corresponding to the portions associated with the fluid layer's rigid rotation and relative motion with respect to the solid Earth, respectively.

[7] In the second, so-called torque, approach, the interaction torque between the fluid layer and the solid Earth is computed from the GCM output. The effect on the Earth rotation is evaluated dynamically from the torque:

$$\frac{d\mathbf{H}_{\text{solid Earth}}}{dt} = \mathbf{\Gamma}_{\text{fluid layer}}, \tag{2}$$

where $\mathbf{\Gamma}$ is the total torque associated with the action of the fluid layer on the solid Earth.

[8] The two approaches are linked by the angular momentum budget equation of the fluid layer, which is a direct consequence of the action/reaction principle:

$$\frac{d\mathbf{H}_{\text{fluid layer}}}{dt} = -\mathbf{\Gamma}_{\text{fluid layer}} \tag{3}$$

The two approaches are, in principle, equivalent, but the torque and the angular momentum are computed independently from different parameters within the model output. Numerically, the approaches usually differ somewhat, mainly in the axial component [see *de Viron et al.*, 2001]. The discrepancy is usually blamed on the torques, as their computation is more delicate than that of the angular momentum.

[9] In section 2 we give some information about the model used and the torque computation. In section 3 we test the validity of the computation. In section 4 we will show the relative magnitude of the different terms of the angular momentum budget equation. Section 5 shows effects of the atmosphere on Earth rotation and utilizes a wavelet analysis to examine the temporal and frequency variability of parameters, and section 6 is devoted to conclusions.

2. Data Used and Torque Computations

[10] In our study, we use a set of results from a run throughout the twentieth century using the global circulation model (GCM) from the UK Hadley Centre, forced by sea surface temperatures and global ice conditions, to evaluate the effect of the atmosphere. The model is described by *Rowell* [1998], and results here are part of efforts within the Climate of the 20th Century Project. Monthly mean values of sea ice and sea surface temperature during the period since February 1870 have been used as boundary conditions to drive the model, which, like all such models, is based on the equations of motion, energy, and continuity for the global atmosphere, including modeling the physics of atmospheric moist processes. The atmospheric model is allowed to run for this period, producing, among other parameters, values of winds through the depth of the atmosphere on a three- dimensional global grid and surface pressures on a two-dimensional global grid, which are the basis of the angular momentum excitation functions. The model motion term of the axial atmospheric angular momentum (AAM) was analyzed by *Rosen and Salstein* [2000], who focused on the modulation of interannual variability. Using these basic quantities and ancillary information from the model, including its topography field, excitations for angular momentum and values of torque components are produced. We compare the Hadley Centre model with the National Center for Environmental Prediction/National Center for Atmospheric Research (NCEP/NCAR) reanalysis [*Kalnay et al.*, 1996], which in addition to boundary forcing has assimilated the heterogeneous variety of atmospheric data that were available since 1948 to form similar fields and from which we also compute the angular momentum and torque values that we present here.

[11] From this model, we used 10 two-dimensional fields: surface pressure, the local contribution to the atmospheric angular momentum (AAM) (matter and motion terms for three components), friction drag (two tangential components), and the constant topography. All the time-varying fields are provided every month between 1870 and 1998.

[12] The torque is computed as by *de Viron et al.* [2001]: three torques have been considered, a mountain torque acting on the topography, a gravitational torque due to the interaction between the mass in the atmosphere and in the Earth, and a friction torque. Of the gravitational torque, only the part associated with the Earth form factor (J_2) is computed. As the topography is given with respect to the geoid, the non-J_2 part is already included in the mountain torque. As explained by *Bell* [1994], the mountain torque acting on the Earth bulge is proportional to the gravitational torque on J_2, and we have

$$\mathbf{\Gamma}_E = \mathbf{\Gamma}_{\text{pressure}\rightarrow\text{bulge}} + \mathbf{\Gamma}_{\text{gravitation}\rightarrow\text{J}_2} = \mathbf{\Omega} \wedge \mathbf{H}_{\text{matter}}, \tag{4}$$

where $\mathbf{\Omega}$ is the Earth's mean rotation vector.

[13] The remaining part of the mountain torque is computed using

$$\mathbf{\Gamma} = a^2 \int\int P \left[\frac{1}{\sin\theta} \frac{dh(\theta,\lambda)}{d\lambda} \begin{pmatrix} \cos\lambda\cos\theta \\ \sin\lambda\cos\theta \\ -\sin\theta \end{pmatrix} + \frac{dh(\theta,\lambda)}{d\theta} \begin{pmatrix} \sin\lambda \\ -\cos\lambda \\ 0 \end{pmatrix} \right] \sin\theta \, d\theta \, d\lambda, \tag{5}$$

where θ is the colatitude, λ is the longitude, $h(\theta, \lambda)$ is the topography, P is the surface pressure, and a is the Earth mean radius. The friction torque is simply computed by integrating the cross product of the position vector and the local friction drag on the Earth's surface.

3. Torque and AAM Testing

[14] In order to test the quality of the torque and angular momentum computations, three different methods can be

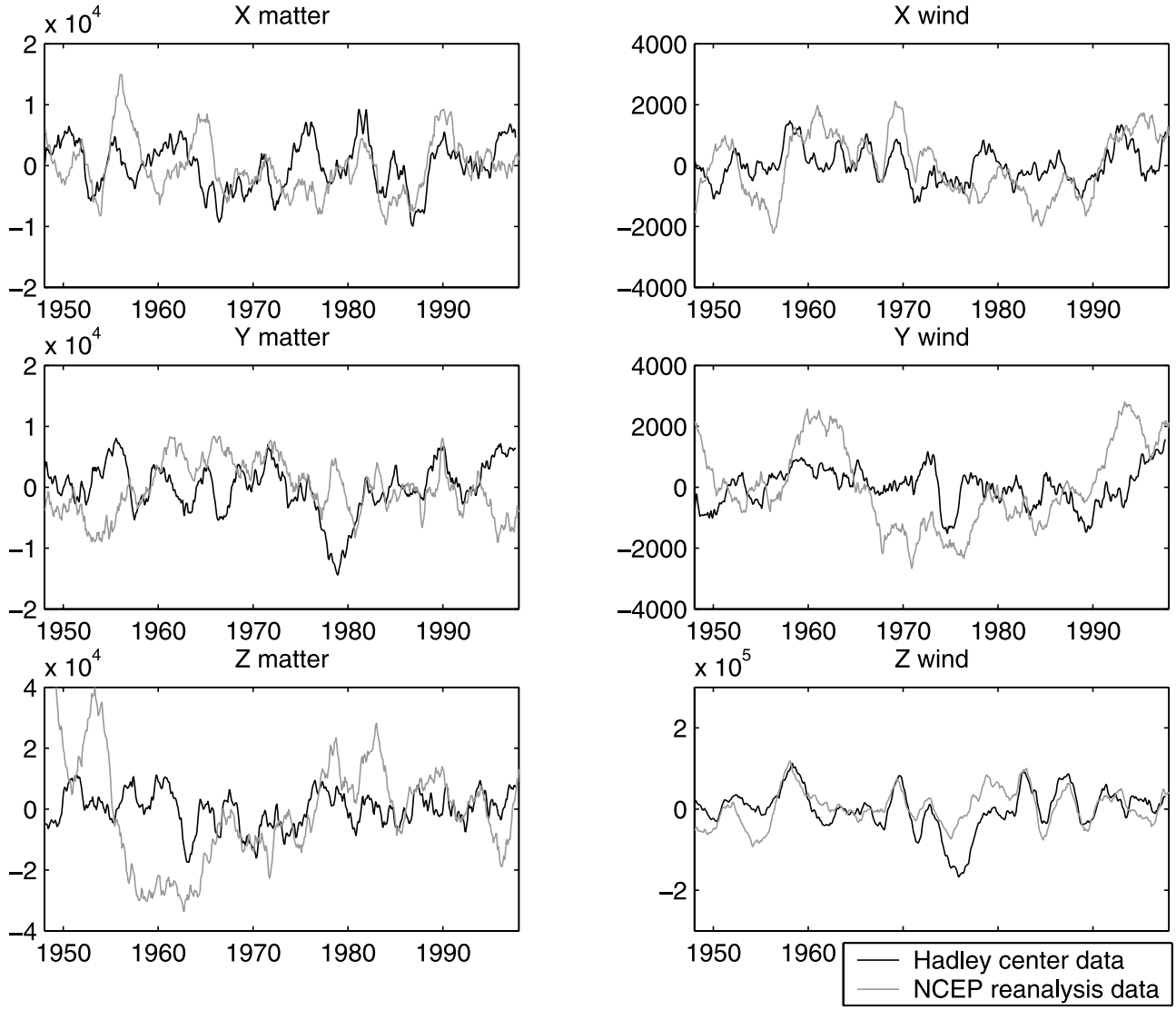

Figure 1. Time series (with a composite seasonal cycle removed, smoothed with a 1-year window and detrended) of the two components of the angular momentum, for the Hadley Centre model (black) and the NCEP reanalysis (gray).

used: (1) the momentum quantities can be compared with the equivalent observed Earth rotation parameter, (2) the computation can be compared with those from another model, and (3) the angular momentum budget equation of the fluid can be tested by using equation (3).

[15] Method 1 is not appropriate here because the dynamic effects are not limited to atmosphere-Earth interactions for many timescales of interest here. For LOD the effect of the core is thought to be much larger, but its value is not known with a sufficient precision to allow residual computation [see *Ponsar et al.*, 2003]. For polar motion the ocean effect is not known for such a long timescale, and it is at least as comparable to the atmospheric effect as for higher frequencies. The contribution of the core for polar motion may, moreover, be important, though its level is currently unknown. The impact of postglacial rebound effect on the mass distribution may have an impact at the lower frequencies as well. Nevertheless, the comparisons between the contributions of the atmosphere and solid Earth are valuable for the purposes of verifying that the order of magnitude is not too large.

[16] The time series (with a composite seasonal cycle removed, smoothed with a 1-year window and detrended) of the two components of the angular momentum for the Hadley Centre model (black) and the NCEP reanalysis (gray) are given in Figure 1. The series are overall not similar for the two models, mostly for the matter term, but the correlation is high during some episodes. The best correlation is for the axial term and to a lesser extent X wind term. Figure 2 shows a similar comparison for the torque time series. The two model results are uncorrelated for the mountain torque along the Y component, though the friction torque does show a fair correlation. For the X component, there is a slight correlation between the results from the two models, a bit better for the mountain torque than for the friction torque. The axial torque correlation is better than that of the equatorial torque. Table 1 gives the correlation coefficients between the series,

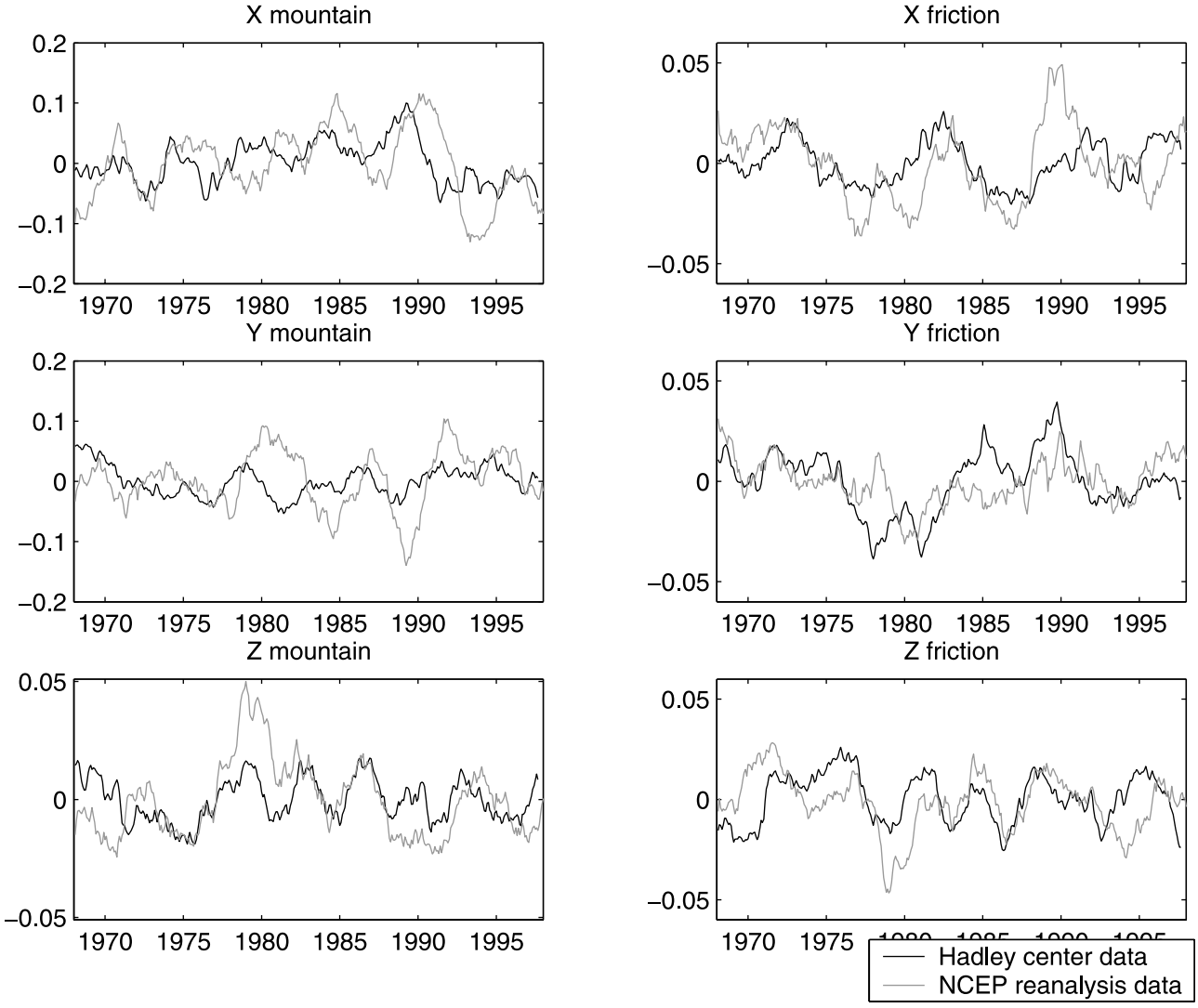

Figure 2. Time series (with a composite seasonal cycle removed, smoothed with a 1-year window and detrended) of the two components of the atmospheric torque, for the Hadley Centre model (black) and the NCEP reanalysis (gray).

together with an estimate of the significance of the coefficients. It can be seen that the correlation at the 90% level (or better) is reached for 7 out of 12 series. Globally, the local torques have higher correlations than the angular momentum, especially than the matter term. This result makes modeling the equatorial component difficult, as most of its signal derives from the ellipsoidal torque which is proportional to that term. For the Z component the wind term is the dominant one, and its good results are reassuring.

[17] Figure 3 shows the angular momentum budget (torque and AAM time derivative) for all three components, smoothed in a 40-month window. As explained by *de Viron and Dehant* [2003], the test is not rigorous enough for the equatorial component if the ellipsoidal effect is kept in the budget, as a common term in both sides of the equations (3) dominates at the 90–95% level (as can be seen from the comparison between Figures 3 (left) and 3 (right)). For the X component the budget is very nearly closed both with and without the ellipsoidal effect. Conversely, for the Y component, only the budget with the ellipsoidal effect is verified. This result is not surprising at all, as the mountain torque, which accounts for a larger part of the nonellipsoidal equatorial torque [see *de Viron et al.*, 2001], is not very accurate as shown by the correlation with the NCEP values. Note that the correlation only considered the end of the data set, when the quality of the AAM budget improves. The budget for the axial component is out of balance; the torque shows low-

Table 1. Correlation Coefficient Between AAM and Torque From the NCEP and HADLEY Models

	X	Y	Z
Mountain torque	0.46[a]	0.16	0.46[a]
Friction torque	0.41[a]	0.43[a]	0.24
Matter AAM	−0.05	0.02	−0.08
Wind AAM	0.44[a]	0.42[b]	0.76[c]

[a]Coefficient is significant at the 90% level.
[b]Coefficient is significant at the 95% level.
[c]Coefficient is significant at the 99% level.

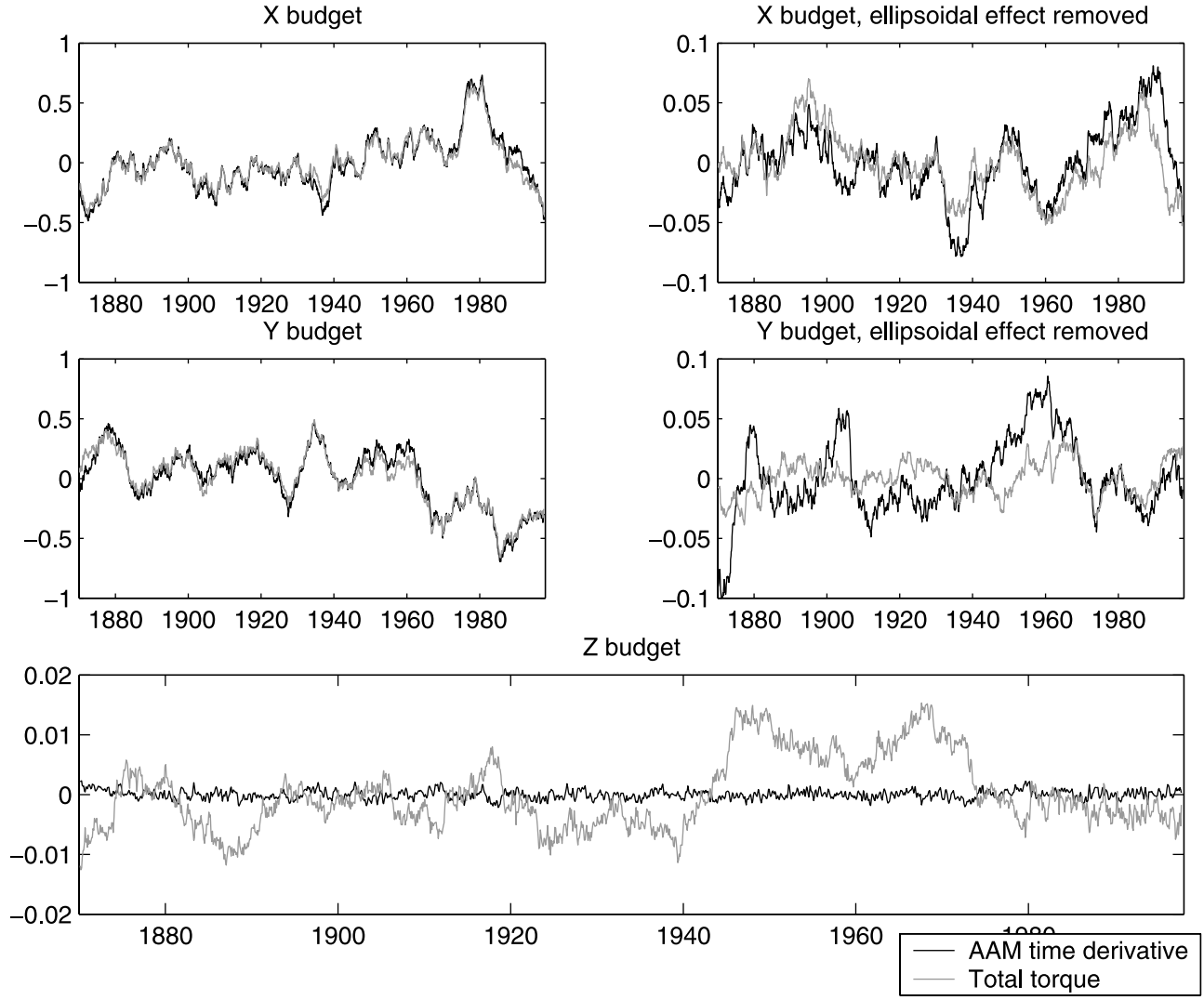

Figure 3. Angular momentum budget (torque and AAM time derivative) for the three components, smoothed with a 40-month window.

frequency variations that do not appear in the AAM time derivative and are likely spurious. To summarize the testing results, we can be most confident about the axial AAM, but the other results needed to be considered more cautiously, so that only an order of magnitude consideration should be inferred here.

4. Results

4.1. Relative Magnitude of the Considered Effect

[18] Figure 4 shows the different torques, with relative magnitudes, normalized so that the sum is 1, for the Hadley Centre model (solid line) and for the NCEP reanalysis (dotted line) for periods ranging from 0 to 60 years. As expected from previous studies [e.g., *Bell*, 1994], the equatorial component is dominated within the whole frequency range by the ellipsoidal torque (associated with the bulge). The mountain and friction torques contribute to a comparable extent to the equatorial components, the mountain torque being slightly larger at periods smaller than about 10 years. Note that at periods between 5 and 6 years, there is a particular period (different for X and Y) at which the relative magnitude of the ellipsoidal torque is not as dominant as elsewhere. In the axial component, mountain and friction torques contribute similarly to the total, alternating with relative significance at different frequencies.

[19] The relative importance of the torques is also different, though some similarities can be observed between the results from the Hadley Centre model and the NCEP/NCAR reanalyses and particularly for the axial component. At low frequency the relative importance of the mountain torque is larger within the NCEP reanalyses. Of course, this result is only an indication because the time considered in each case is different for each series.

[20] Figure 5 shows the same results for the matter and wind terms of angular momentum. It can be observed that for a period smaller than 10 years the data sets have comparable results. For a period longer than 10 years, results from the Hadley Centre and NCEP are in disagreement for both the torques and angular momentum. As expected, the equatorial components are dominated by the

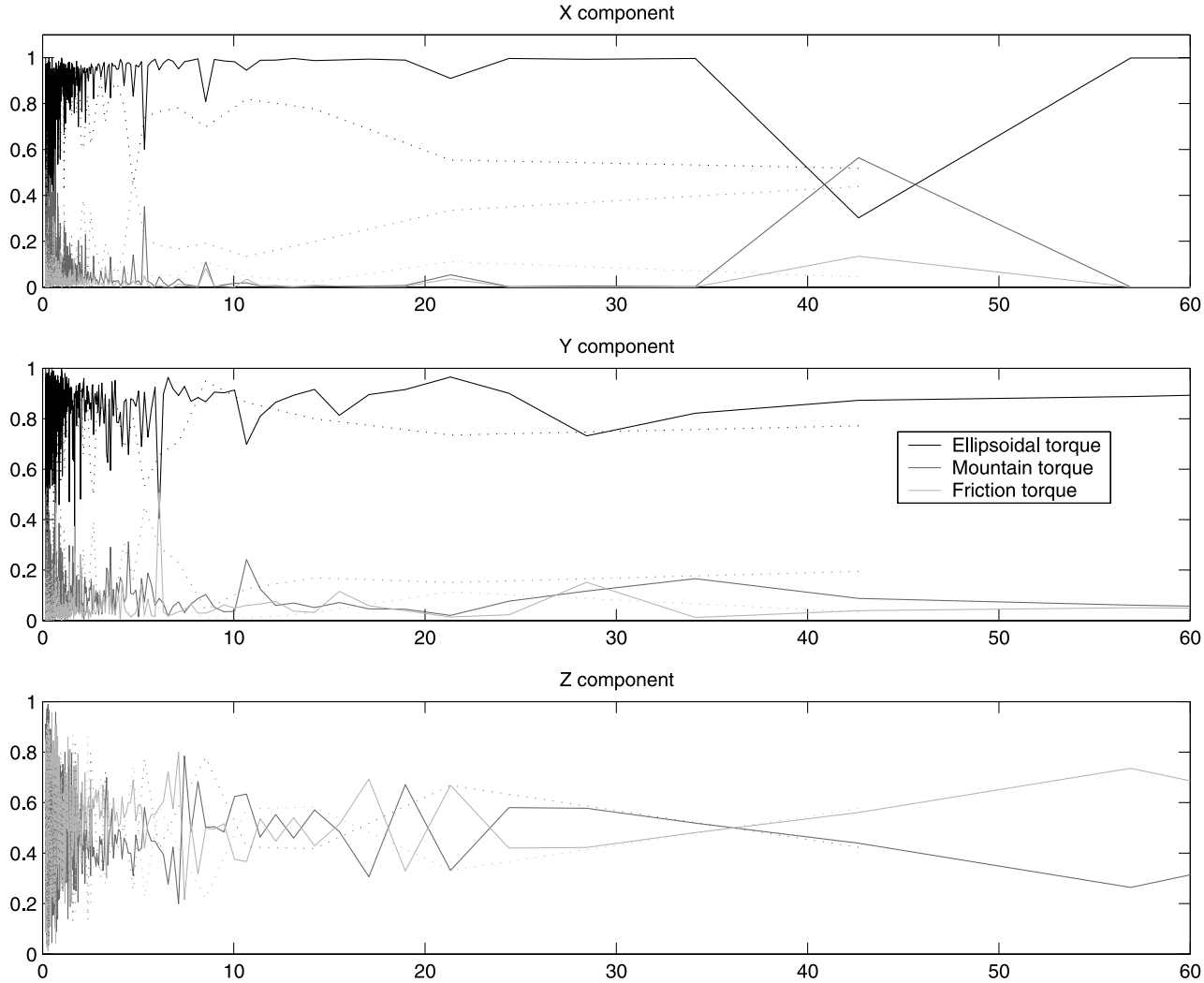

Figure 4. Relative magnitude (normalized such that the sum is 1) of the different torques for the Hadley Centre model (solid line) and for the NCEP reanalysis (dotted line) as a function of the period (year).

mass term, and the zonal component is dominated by the wind term.

4.2. Effect of the Atmosphere on the Low-Frequency LOD

4.2.1. Long-Period Atmospheric Excitation of the LOD

[21] At seasonal scale the variations of the Earth rotation rate, LOD, are more than 95% accounted for by the axial AAM. Nevertheless, the origin of the longer-period oscillations, as, for instance, between 12 and 15 years, has not been firmly identified. Besides the electromagnetic coupling between the bottom layer of the mantle and the fluid core, there may be atmospheric effects associated with a solar influence at the 11-year scale. Such have been investigated by *Abarca del Rio et al.* [2003] including modulations of shorter-period signals. The present quality of the core angular momentum series [see *Ponsar et al.*, 2003] shows that the core seems to be the largest contributor, but it does not rule out an atmospheric and/or oceanic effect. Information from AAM at this band is suggestive, but that derived from the torques are more difficult about which to make conclusions and so will not be treated here.

[22] Let ΔLOD be the variation of the mean solar day with respect to the nominal value LOD = 86,400 s Temps Atomique International (TAI), let H_3 be axial AAM, split in the matter term H_3^m and the wind term H_3^w. By taking into account the increment of inertia of the solid Earth induced by the atmospheric loading, the axial part of the linearized Euler-Liouville equations provides [*Barnes et al.*, 1983]

$$\frac{\Delta \mathrm{LOD}}{\mathrm{LOD}} = \frac{0.70 H_3^m + H_3^w}{C\Omega}, \tag{6}$$

where C is the axial moment of inertia of the Earth (value recommended by the International Association of Geodesy in 1999 is $C = 8.0365(2) \times 10^{37}$ kg m^2).

[23] The left-hand side of equation (6) is the axial geodetic excitation:

$$\chi_3^G = \frac{\Delta \mathrm{LOD}}{\mathrm{LOD}},$$

and the right-hand side is the axial atmospheric excitation χ_3^A.

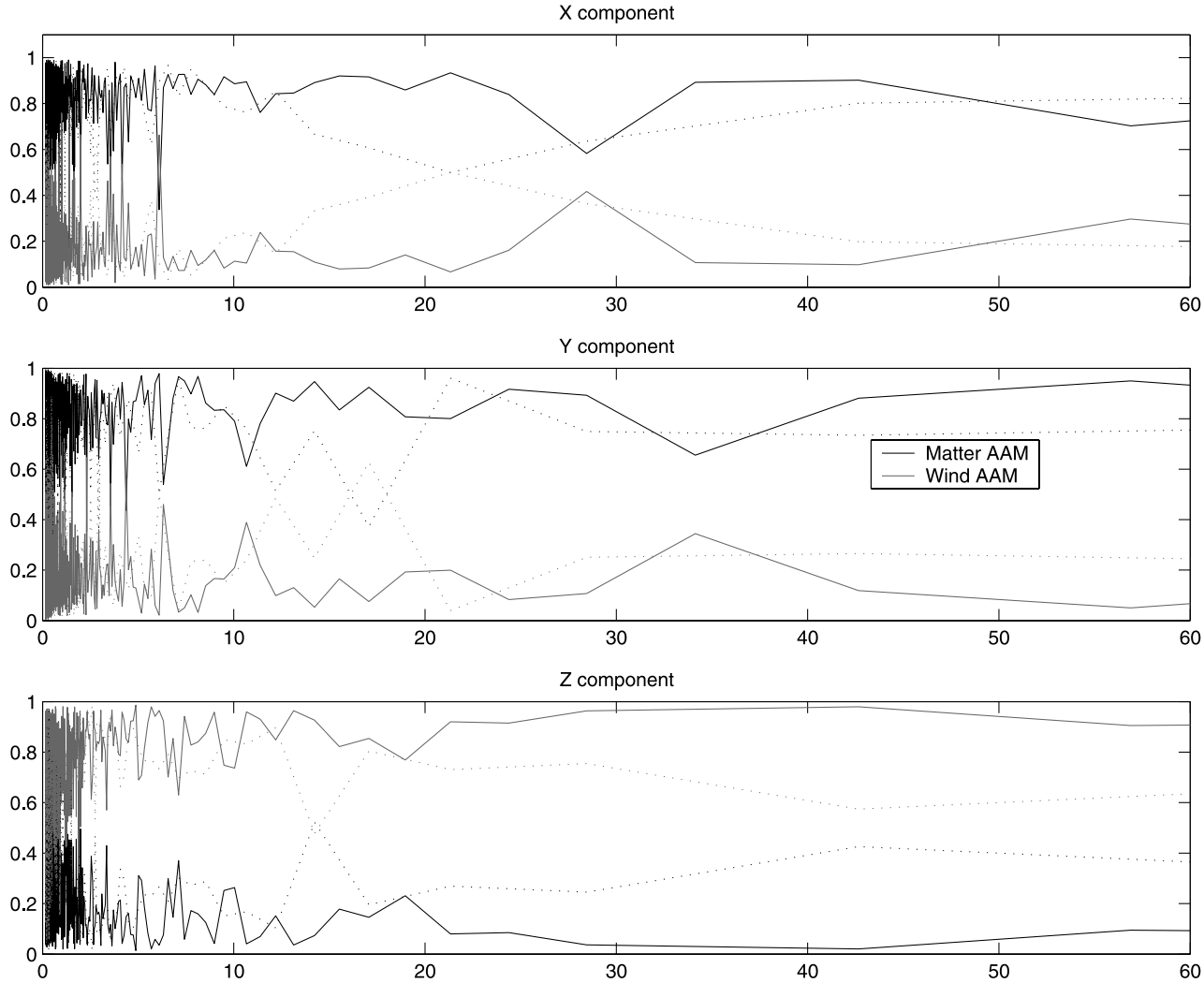

Figure 5. Relative magnitude (normalized such that the sum is 1) of the matter/wind terms of the AAM for the Hadley Centre model (solid line) and for the NCEP reanalysis (dotted line) as a function of the period (year).

[24] When the axial atmospheric torque Γ_3 is considered instead of axial AAM, the atmospheric excitation function has to be reconstructed by integration:

$$\chi_3^A(t) = K - \int_{t_0}^{t} \frac{\Gamma_3}{C\Omega} dt, \tag{7}$$

where K is an unknown integration constant.

[25] For the LOD data we have considered the yearly combined time series computed by R. Gross (Jet Propulsion Laboratory), ranging from 1832 to 1998 and available on the Web site of the International Earth Rotation Service (IERS) Earth Orientation Center (http://hpiers.obspm.fr/eop-pc/products/longterm/longterm.html). This series presents typical accuracy of 0.5 ms in 1870, 0.3 in the 1950s, 0.1 ms from 1960 to 1980, and, thanks to the break through of VLBI, around 0.02 ms in the 1990s. By dividing these quantities by 86,400,000 ms, they also give estimates of the uncertainty for axial excitation function in radians: 5×10^{-9} rad in 1870 and a fortiori smaller after, that is, much less than the uncertainty spoiling atmospheric angular momentum function. Note that the LOD data have been interpolated at the dates of the atmospheric data.

[26] Correlation by frequency band is quantified by the coherence function, displayed in Figure 6 for the axial excitation between 2 years (0.5 cycles per year (cpy)) and 25 years (0.04 cpy) (geodetic/AAM-geodetic/torque). The coherence for subdecadal periods is irregular. On the other hand, significant levels of coherence, above 0.5, are reached for decadal variations, more exactly in the bands [9–12] years, [13–23] years, but there is lack of atmospheric power except for 10 years (AAM power $0.25\chi_3$) and 13–14 years (AAM power $0.2\chi_3$). A more accurate comparison is obtained by fitting a 14-year sinusoidal component in the LOD and the corresponding atmospheric contribution. Over the epoch 1870–1997, the 14-year component of the LOD (2.6 ms) would be partly accounted by the atmosphere up to 0.6 ms, that is, 20% of the power in LOD at this period (phases of which are consistent as expected from the coherent analysis above). Additionally, we found an observable secular effect in the LOD, at the level of 80 μs/

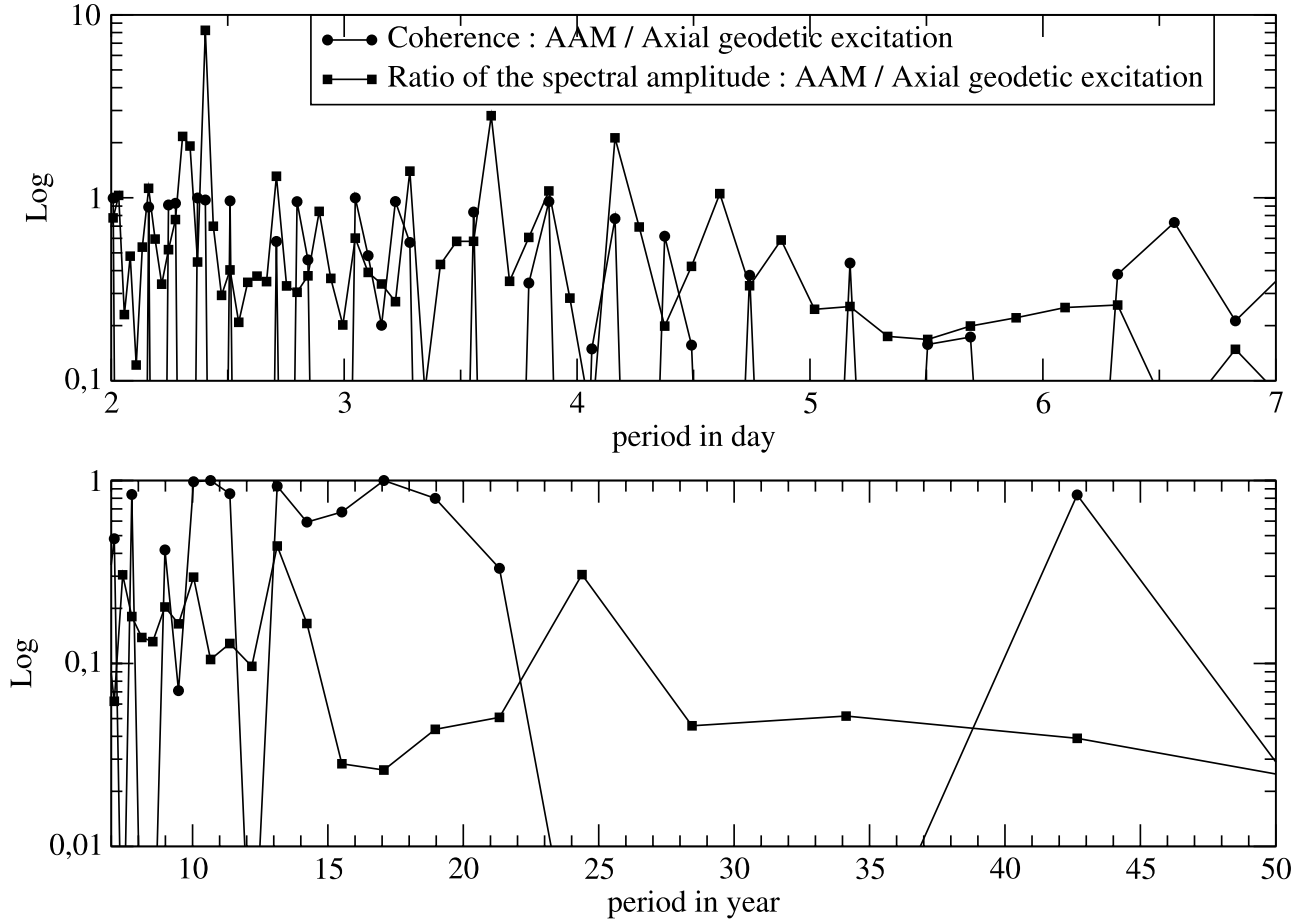

Figure 6. Coherence between axial atmospheric and geodetic excitation functions and ratio of the spectral amplitudes. The case of the axial torque is not displayed because its strong variability is suspect.

century, which is nevertheless much smaller than the observation (see Table 2).

[27] This lack of power is not surprising, as it is expected that the low-frequency LOD variation are dominated by the core/mantle interaction effect. More surprising is the coherence between the two series. This may be related to some already documented facts: *Lambeck and Cazenave* [1976] noted the connection between global temperature and LOD, and *Raisanen* [2003] showed that there is a correlation between the global mean pole-to-equator temperature gradient and global AAM, though with an amplitude about 1 order of magnitude too small to explain the decadal LOD variation. Those bits of information, together, imply that the AAM would be coherent with the low-frequency LOD but with a power much too small.

4.2.2. Time-Variable Atmospheric Excitation of the Low-Frequency LOD

[28] Wavelet analysis is now a well-accepted tool allowing the investigation of the time-variable frequency content of a time series. Some theoretical and technical considerations are given in Appendix A. We applied this analysis to the axial atmospheric torque and angular momentum. We used a mother wavelet of the Morlet type. A first application of this analysis on data time series equally spaced at 1-month interval did not show any unexpected feature at any component besides the very well known annual contribution. Although, in the case of the axial component the contribution at half a year and shorter periods appears as significant. The scales can be associated with a corresponding frequency. Adopting $\omega_0 = 6$ for Morlet wavelet (see equation (A1)), the frequency(s) is approximately equal to the Fourier period (P) (P = 1.03 s). The choice of the factor "width" (see equation (A2)) depends on the width in the spectral space of the wavelet function. The largest width we could use for Morlet wavelet, still keeping an adequate sampling in space, is 0.5. The smaller the width factor, the smaller the resolution. We pick out a width factor of 0.1, given thus a maximum of 61 scales from 2 years to 128 years. (according to expression (A2)) For this analysis we only plot 41 scales from 2 to 32 years.

[29] Figure 7 shows the wavelet analysis for the axial AAM. Values in wavelet power spectrum are normalized by $1/\sigma^2$, where σ is the data time series variance. In order to test the robustness of our results we investigate the significance of the peaks with respect to a peak coming from the random error on the computed/modeled quantities. In that sense, only local peaks above the 95% confidence interval will be considered.

Table 2. Secular Effect on the Polar Drift and Length of Day

	x, mas/century	y, mas/century	LOD, mas/century
AAM	−7	−5	0.08
Torque	−9	−6	too strong
Observed	134	−267	1.80

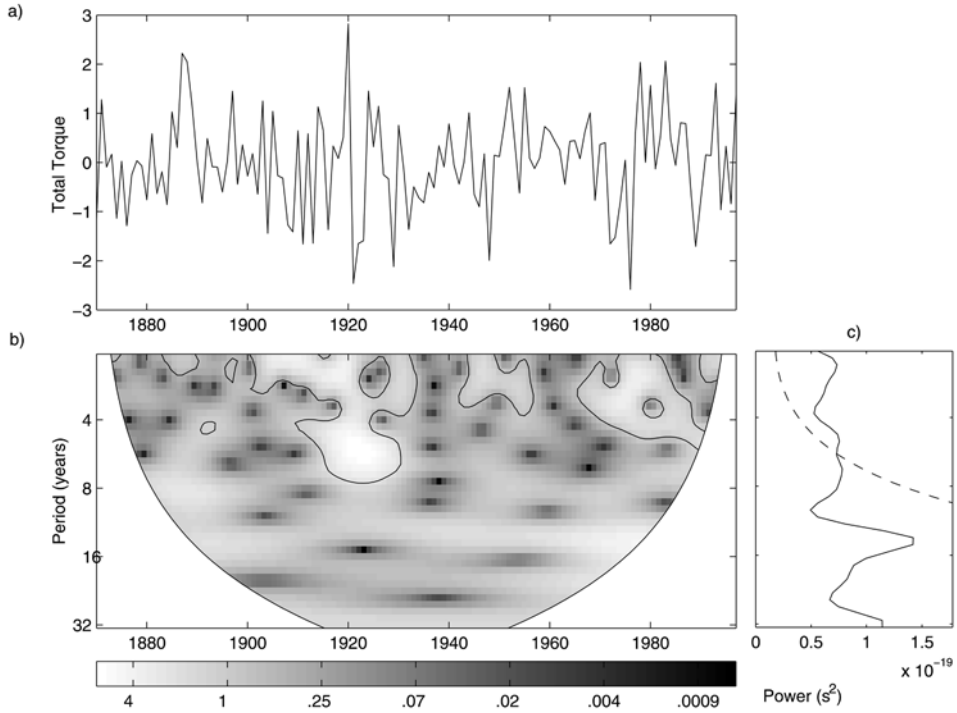

Figure 7. Wavelet transform of the axial torque (a) Component of the total torque time series. (b) Wavelet power spectrum using Morlet as mother wavelet. The black contour is the 95% confidence level. (c) Global wavelet spectrum for the component of the total torque.

[30] Regarding Figure 7, only the contribution with periods shorter than 5 years appears to be significant. Particularly, it is not surprising to find a significative contribution at El Niño frequency band. It is an additional confirmation of the good correlation between the axial component of the friction and mountain torques and El Niño-Southern Oscillation cycle [*de Viron et al.*, 1999].

[31] Considering longer-period variations, the time variability of the low-frequency atmospheric contribution to LOD is less than globally significant. Similar conclusions can be drawn for the wavelet spectrum of the axial torque (not shown), very similar to the axial torque wavelet spectrum.

4.3. Effect of the Atmosphere on the Polar Motion

4.3.1. Long-Period Atmospheric Excitation of the Polar Motion

[32] The motion of the rotation axis in the plane tangential to the north pole is driven mostly by exchanges of equatorial angular momentum between the atmosphere, the oceans, and the solid Earth, especially at seasonal periods. However, the atmospheric effect at periods larger than 10 years remains not well characterized. Our 130-year-long AAM and torque series allow us to investigate those periods. As explained in section 3, the torque and AAM approach give exactly the same excitation at low frequency because of the dominant ellipsoidal effect. Consequently, only the results from the AAM are shown here.

[33] The most common and easiest way for investigating the problem is to compare the atmospheric excitation (torque/AAM) to the total excitation derived from the observed polar motion. In particular, this method allows us to get rid of the Chandler wobble resonance in the signal as follows.

[34] Let x_p and $-y_p$ be the coordinates of the celestial intermediate pole in the terrestrial frame, and let us define the complex-valued quantity $p = x_p - iy_p$. Notice that p also represents the terrestrial coordinates of the rotation axis at the timescale considered in this study. Let $H = H_x + i\,H_y$ be the equatorial components of the AAM, split into the matter term H^m and the motion term H^w.

[35] For periods longer than a few days the angular momentum balance, applied to the system constituted by the fluid layer and the solid Earth and expressed in the terrestrial frame, gives, to first order, the linearized Euler-Liouville equation. Then by assuming an elastic mantle decoupled from the fluid core, we obtain the following differential equation for the polar motion [*Brzeziński*, 1994]:

$$p + \frac{i}{\sigma_{cw}}\frac{\mathrm{d}p}{\mathrm{d}t} = \frac{H^m + 1.43H^w}{(C_m - A_m)\Omega}, \tag{8}$$

where $\sigma_{cw} = \sigma_0(1 + i/2Q)$ is the complex-valued frequency of the Chandler wobble, known as a damping process of frequency $\sigma_0 = 0.8435$ cycle per year (cpy), and quality factor $Q = 179$ according to *Wilson and Vicente* [1990]. The chosen value is not important for our study, as we focus on long timescales. C_m and A_m are the axial and the equatorial moments, respectively, of inertia of the mantle (values recommended by the International Association of Geodesy in 1999: $C_m = 7.0400 \times 10^{37}\,\mathrm{kg\,m^2}$, $A_m = 7.0165 \times 10^{37}\,\mathrm{kg\,m^2}$). Ω is the mean value of the Earth angular velocity as adopted in the IERS numerical standards: $\Omega = 7.2921150 \times 10^{-5}$ rad s^{-1}.

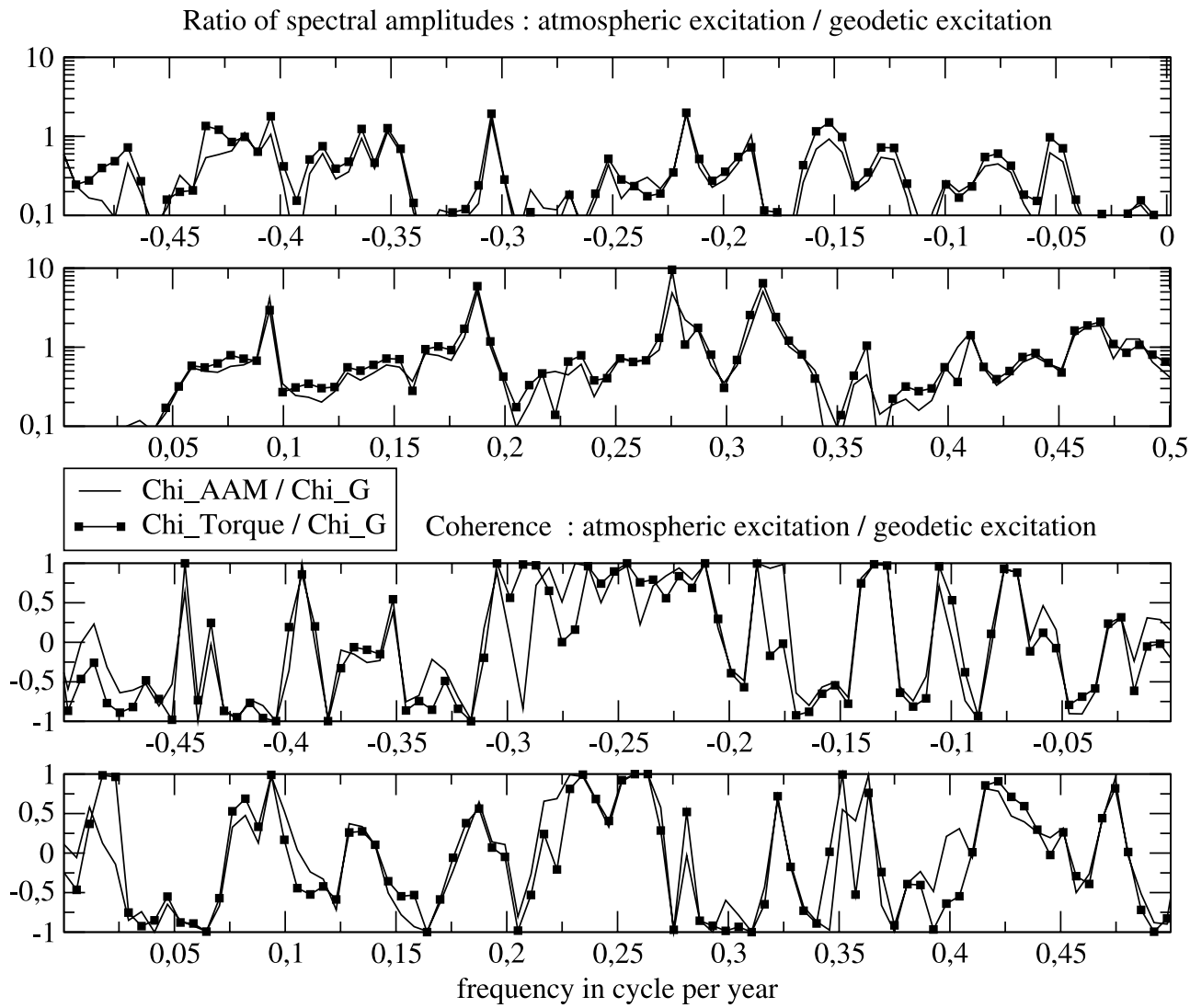

Figure 8. (bottom) Coherence between equatorial atmospheric and geodetic excitation functions and (top) ratio of the spectral amplitude.

[36] The left-hand side of equation (8) is the equatorial geodetic excitation

$$\chi^G = p + \frac{i}{\sigma_{cw}} \frac{\mathrm{d}p}{\mathrm{d}t}. \tag{9}$$

The right-hand side of expression (8) constitutes the equatorial atmospheric excitation:

$$\chi^A = \frac{H^{mat} + 1.43H^w}{(C_m - A_m)\Omega}. \tag{10}$$

When atmospheric torque $\Gamma = \Gamma_x + i\,\Gamma_y$ is considered instead of AAM, the equatorial atmospheric excitation function to be used is

$$\chi^A_T = i(1.13\Gamma - 0.136\Gamma_E)\frac{1}{A\Omega\sigma_{cw}}, \tag{11}$$

where A is the equatorial moment of inertia of the Earth (value recommended by the International Association of Geodesy in 1999: $A = 8.0101 \times 10^{37}$ kg m^2). Γ_E is the component of the atmospheric torque associated with the ellipsoidal shape of the Earth (pressure and gravitational effects). This expression can been derived from theoretical considerations exposed by *de Viron* [1999] and has been already applied for computing the atmospheric effect on polar motion [*Bizouard et al.*, 1999] from torque series.

[37] For the polar motion (PM) data we have considered the combined time series C01, sampled at 0.05 year interval, produced by the IERS Earth Orientation Center (http://hpiers.obspm.fr/eop-pc/products/combined/eopcomb.html). Typical accuracy is 80 mas in 1870, 20 mas from 1900, 10 mas from 1960, and 0.2 mas from 1980. After interpolation at the dates of the atmospheric data, geodetic equatorial excitation is computed by taking discrete second order approximation of the PM time derivative. The expected accuracy follows the PM ones.

[38] The relationship between series at different frequency bands is quantified by the coherence function, displayed in Figure 8, from 2 years (0.5 cpy) to 25 years (0.04 cpy)

Table 3. Frequency Bands or Peaks Where the Coherence Between Observed Equatorial Excitation and Atmospheric Excitation is Significative (Above 0.5)[a]

	$\lvert\chi_A\rvert/\lvert\chi_G\rvert$			
	1	2–3	4–6	>9
Prograde	2–2.1*y*		3.1*y*	3.7–4.7*y*
	2.3–2.4*y*		5.3*y*	
	2.7*y*		10.7*y*	
Retrograde	−2.2*y*	−3.3*y*		
	−2.6*y*	−4.6*y*		
	−5.3*y*			

[a]We give the approximative ratio of their amplitude $\lvert\chi_A\rvert/\lvert\chi_G\rvert$.

(geodetic/AAM to geodetic/torque). Below 20 years, significative coherence (above 0.5) as well as satisfactory agreement in power (above 0.5) are noticable for a number of periods, as shown in Table 3. According to our results the atmospheric effect on the slow polar motion is very small at periods longer than 10 years, at the level of a few milliarc seconds.

[39] The least squares fit of the same harmonics in polar motion reveals fluctuations at least 3/4 times larger and is out of phase. Consequently, even if we cannot explain the Markowitz wobble from the Earth-atmosphere excitation, we show that very slow polar motion variations can be excited by the atmosphere dynamics above the precision level of the observation (see Table 2). Additionally, as we mentioned, the conclusion from this study is more qualitative than quantitative: As the order of magnitude of the atmospheric excitation is close to the right order of magnitude, we cannot rule out an excitation of the Markowitz wobble by the atmosphere.

4.3.2. Time-Variable Atmospheric Excitation of the Low-Frequency Polar Motion

[40] Again, we investigate any significant time-variable low-frequency atmospheric excitation of the polar motion. Figures 9 and 10 show the wavelet analysis for the equatorial components of the total atmospheric torque (mountain plus friction plus elliptical), normalized by $1/\sigma^2$, where σ is the data time series variance.

[41] As for the axial component, only contributions with periods shorter than 5 years appear to be substantial. Considering decadal and longer-period variations, the total torque contributions are again not significant. Despite the fact that a local wavelet power spectrum peak exists at 12–15 years for the equatorial components, it is not significant: in the plot of the *x* component of the torque, the peak (12–15 years) is significant (local and global wavelet power spectrum), but in the case of the *y* component of the equatorial torque the peak is significant locally but less than significant globally. Furthermore, the possible contribution to the Markowitz wobble is below the cone of influence. So that, contaminated by the edge effect, this local spike is not significant at all and is undistinguishable from a random noise feature, results that support those of section 4.2.

5. Conclusion

[42] Pressure and friction drag and wind data simulated by a meteorological model of the Hadley Centre have allowed us to compute a 130-year-long time series of atmospheric angular momentum and torque that relate to polar motion and LOD variations. The quality of the series

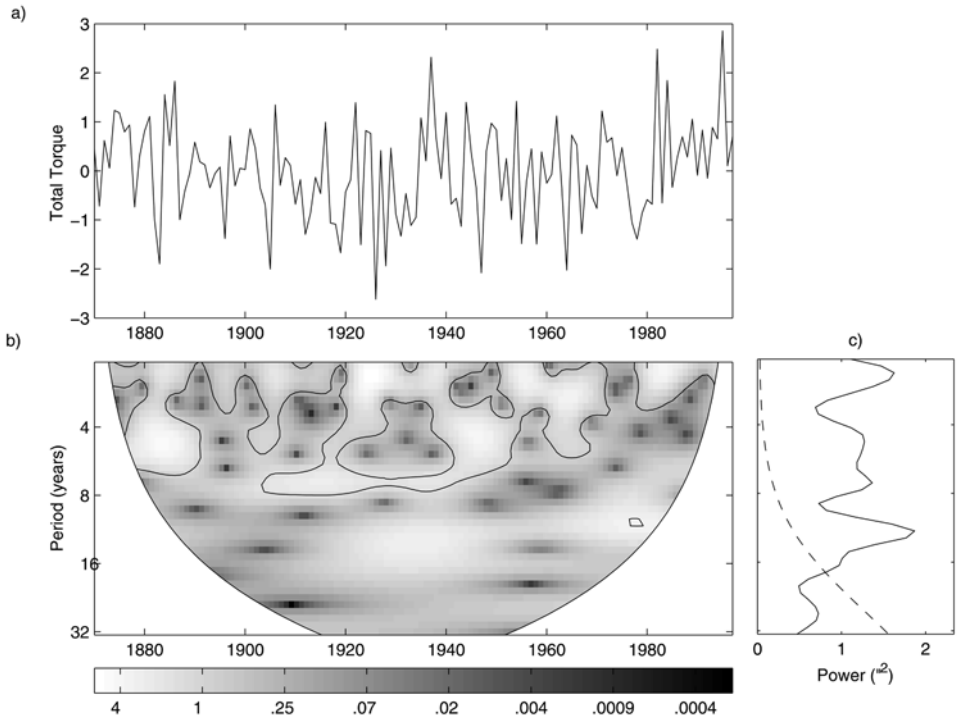

Figure 9. Wavelet transform of the equatorial torque (*x* component) (a) Component of the total torque time series. (b) Wavelet power spectrum using Morlet as mother wavelet. The black contour is the 95% confidence level. (c) Global wavelet spectrum for the component of the total torque.

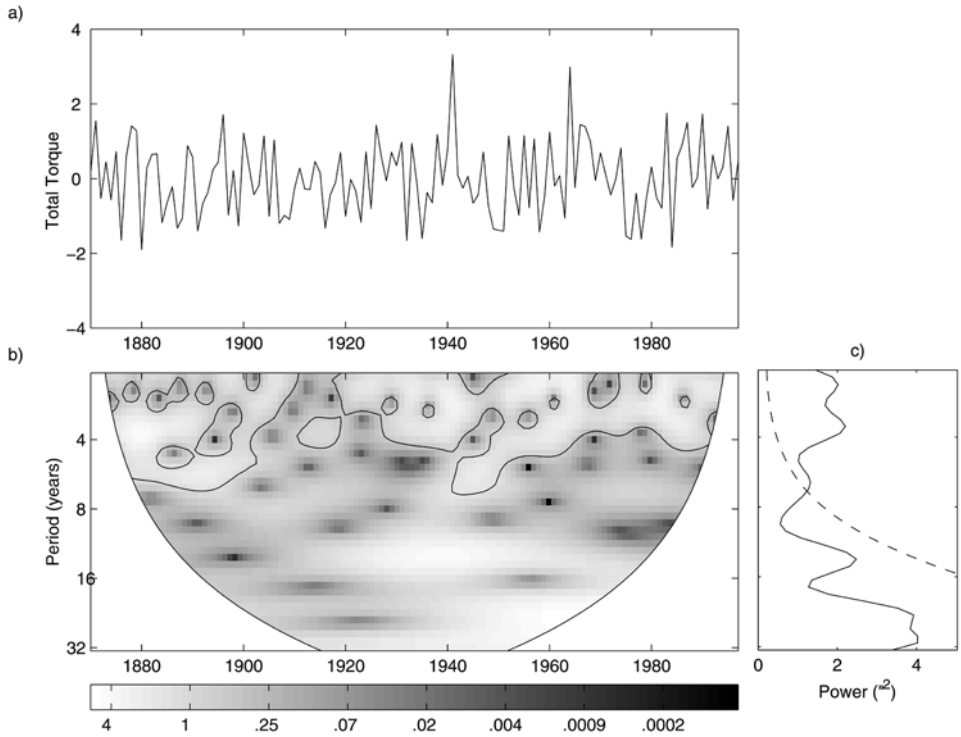

Figure 10. Wavelet transform of the equatorial torque (*y* components). (a) Component of the total torque time series. (b) Wavelet power spectrum using Morlet as mother wavelet. The black contour is the 95% confidence level. (c) Global wavelet spectrum for the component of the total torque.

has been tested from comparisons with assimilated AAM series on overlapping spans (1948–1997). Whereas equatorial components appear to be more difficult to model, axial AAM seems reliable.

[43] Globally, the simulated atmospheric excitation does not account for the long-term irregularities of the Earth's rotation (with those longer than 10 years), but we noted a secular increase of the length of day by about 5% of the observed rate, a polar drift of 10 mas/century in the direction 146°W (the observed drift is 331 mas/century toward 76°W [see *Schuh et al.*, 2001]), as well as decadal variation of polar motion (10 years). According to our results the atmospheric excitation of the Markowitz wobble is not sufficient to explain the observations.

[44] However, we notice that the decadal variation in axial atmospheric excitation is strongly coherent with that of the LOD and accounts for 20% of the amplitude of the 13–14 years harmonic in LOD. Subdecadal variability in the axial AAM results shows increased variability in recent years. Moreover the PM should be excited at the level of 2–3 mas at 25 cpy and −20 cpy.

[45] Because of the results are based on simulations driven by a model dynamics whose boundary conditions are the records of sea surface temperature throughout the century, results may depend on the data sets used to drive them and the natural variability of the model. Indeed, *Rosen and Salstein* [2000], who reported on multiple runs of this type of model, noted a considerable spread of such quantities. Long-term oceanic effects have to also be investigated, and we may be able to do so using coupled atmosphere-ocean models.

Appendix A: Time Series Analysis

[46] Contrary to the classical Fourier transform, the most important feature of the wavelet analysis is the detection of the time-varying amplitudes and frequencies. We used a mother wavelet of the Morlet type, obtained by shifting a Gaussian function in the Fourier space. For geophysical applications it is useful to adopt the complex-valued Morlet wavelet function

$$\psi(t) = \pi^{-1/4}\left(e^{-i\omega_0 t} - e^{-i\,\omega_0^2/2}\right)e^{-t^2/2}, \tag{A1}$$

where in practice, ω_0 often takes $\omega_0 = 5$ [*Daubechies*, 1992]. For this value the second term in the former equation is so small that it can be neglected.

[47] In choosing Morlet as the mother wavelet, we considered the following factors: (1) the Morlet wavelet is nonorthogonal and has been used quite often in analysis of geophysical processes where smooth variations are normally expected [*Foufula-Georgiou and Kumar*, 1994], (2) it is complex, ensuring that we will be able to recover information about both amplitude and phase; and (3) looking for a better resolution in time, we chose a narrow function.

[48] The width of the Morlet wavelet was calculated linked to the choice of a set of scales. According to *Torrence and Compo* [1998] the desired scales are given by

$$\text{scales}_j = s_{\min} 2^{i\,\text{width}}, \tag{A2}$$

where $j = 0, 1, \ldots, \log_2(N\Delta t/s_{\min})/\text{width}$ and $s_{\min}$ refers to the lowest scale we can show in a graphical interface. The

time series is padded with zeroes in order to bring the total length up to the next higher power of two. N is the total number of points after the zero padding. Usually, $s_{\min}$ is selected as $2\Delta t$, where Δt is the time spacing of data.

[49] To test the significance of the wavelet results, we show the global wavelet (GW) spectrum in our wavelet plots. The GW spectrum refers to the time average over all the local wavelet spectra [*Torrence and Compo*, 1998]. This quantity is showed as an indicator of the background spectrum, against which the local peaks could be compared. In that sense, only local peaks above the 95% confidence interval will be considered. To determine the significance levels, it is necessary to make assumptions about the background spectrum.

[50] We assumed that the total atmospheric torque error possesses a red noise spectrum that decreases in amplitude with increasing frequency. *Hasselmann* [1976] demonstrated that a first-order autoregressive process (AR1) is enough to explain the response to a climate system to random forcing, representative of such a red noise spectrum. Let x an autoregressive process of order 1 with coefficient ρ, thus [*Kim and North*, 1998, p. 19]

$$x(t_i) = \rho\, x(t_{i-1}) + \epsilon(t_i), \tag{A3}$$

where ϵ refers to a Gaussian white noise with zero mean and variance σ^2. The average autocorrelation coefficient (ρ) can be expressed in function of the characteristic time scale of the AR process (τ) [*Schultz and Mudelsee*, 2002]

$$\rho = \exp\left[\frac{(t_N - t_1)/(N-1)}{\tau}\right], \tag{A4}$$

where N refers to the total number of points. We applied the TAUEST program [*Mudelsee*, 2002] in order to determine τ and thus ρ for each of the three components of the total atmospheric torque. The respective average autocorrelation coefficients for the total atmospheric torque components are 0.80, 0.55, and 0.69.

[51] The appropriateness of the AR1 parameters thus determined was checked by testing the equality of the power spectrum corresponding to the theoretical autoregressive process and the estimate spectrum of each data time series in the interval $[0, f_{\mathrm{Nyq}}]$. Such a check was performed using nonparametric run test from the REDFIT program [*Schultz and Mudelsee*, 2002, p. 423]. Thus characterized, the respective red noise spectra was used to establish the null hypothesis for the significance level of a given peak in the GW spectra.

[52] The level of significance for a given peak of the wavelet spectrum is considered with respect to a background spectrum (P_B). The P_B is the normalized (by the variance) Fourier power spectrum of the theoretical AR1 process. Thus, once P_B is known and the 95% confidence level for a Morlet mother wavelet is chosen, it is possible to calculate the 95% confidence contour limits at each scale as [*Torrence and Compo*, 1998]

$$\frac{1}{2} P_B \chi^2_2. \tag{A5}$$

[53] **Acknowledgments.** David Rowell of the UK Hadley Centre is acknowledged for providing us with the Hadley Centre atmospheric data. NCEP atmospheric data are from the Climate Diagnostic Center (CDC) of the NOAA (http://www.cdc.noaa.gov). O.de Viron is a postdoctoral researcher of the Belgian Fonds National de la Recherche Scientifique. L. Fernández is a postdoctoral grant holder of the Consejo Nacional de Investigaciones Científicas y Técnicas, CONICET, Argentina.

References

Abarca del Rio, R., D. Gambis, and D. Salstein (2000), Interannual signals in length of day and atmospheric angular momentum, *Ann. Geophys.*, *18*, 347–364.

Abarca del Rio, R., D. Gambis, D. Salstein, P. Nelson, and A. Dai (2003), Solar activity and Earth rotation variability, *J. Geodyn.*, *36*, 423–443.

Ball, R. H., A. B. Kahle, and E. H. Vestine (1969), Determination of surface motion of the Earth's core, *J. Geophys. Res.*, *74*, 3659–3680.

Barnes, R. T. H., R. Hide, A. A. White, and C. A. Wilson (1983), Atmospheric angular momentum fluctuations, length-of-day changes and polar motion, *Proc. R. Soc. London, Ser. A*, *387*, 31–73.

Bell, M. J. (1994), Oscillations in the equatorial components of the atmosphere's angular momentum and torques on the Earth's bulge, *Q. J. R. Meteorol. Soc.*, *120*, 195–213.

Bizouard, C., O. de Viron, V. Dehant, and D. Gambis (1999), Atmospheric effect on polar motion from the torque approach, paper presented at XXIV EGS General Assembly, Session G12, The Hague, Netherlands, 19–23 April.

Brzeziński, A. (1994), Polar motion excitation by variations of the effective angular momentum function, II: Extended model, *Manuscr. Geod.*, *19*, 157–171.

Chen, J. L., C. R. Wilson, B. F. Chao, C. K. Shum, and B. D. Tapley (2000), Hydrologic and oceanic excitations to polar motion and length-of-day variation, *Geophys. J. Int.*, *141*, 149–156.

Daubechies, I. (1992), *Ten Lectures on Wavelets*, *Cbms-Nsf Reg. Conf. Ser. Appl. Math.*, *61*, Soc. for Ind. and Appl. Math., Philadelphia, Pa.

de Viron, O. (1999), Effet de l'atmosphère et de l'océan sur la rotation de la Terre: Aplication numérique au calcul des nutations, Ph.D. thesis, Catholic Univ. of Louvain, Louvain, Belgium.

de Viron, O., and V. Dehant (2003), Test on the validity of the Atmospheric Torques on Earth computed from model outputs, *J. Geophys. Res.*, *108*(B2), 2068, doi:10.1029/2001JB001196.

de Viron, O., V. Dehant, P. Paquet, and D. A. Salstein (1999), El Niño signal in local and global atmospheric torques, *IERS Tech. Note*, *26*, 51–55.

de Viron, O., S. L. Marcus, and J. O. Dickey (2001), Diurnal angular momentum of the atmosphere and its consequences for Earth's nutation, *J. Geophys. Res.*, *106*, 26,747–26,759.

Foufula-Georgiou, E., and P. Kumar (1994), *Wavelets in Geophysics*, edited by E. Foufula-Georgiou and P. Kumar, Academic, San Diego, Calif.

Hasselmann, K. (1976), Stochastic climate models. Part I: Theory, *Tellus*, *28*(6), 473–485.

Kalnay, E., et al. (1996), The NCEP/NCAR 40-year reanalysis project, *Bull. Am. Meteorol. Soc.*, *77*, 431–3471.

Kim, K.-Y., and G. R. North (1998), *Statistical Methods in Climatology*, Clim. Syst. Res. Program, Tex. A&M Univ., College Station, Tex.

Lambeck, K., and A. Cazenave (1976), Long term variation in the length of day and climatic change, *Geophys. J. R. Astron. Soc.*, *46*, 555–573.

Marcus, S. L., Y. Chao, J. O. Dickey, and P. Gégout (1998), Detection and modeling of nontidal oceanic effects on the Earth's rotation rate, *Science*, *281*, 1656–1659.

Mudelsee, M. (2002), TAUEST: A computer program for estimating persistence in unevenly spaced weather/climate time series, *Comput. Geosci.*, *28*, 69–72.

Munk, W. H., and G. F. McDonald (1960), *The Rotation of the Earth, a Geophysical Discussion*, 323 pp., Cambridge Univ. Press, New York.

Ponsar, S., V. Dehant, R. Holme, D. Jault, A. Pais, and T. Van Hoolst (2003), The core and fluctuations in the Earth's rotation, in *Earth's Core: Dynamics, Structure, Rotation*, *Geophys. Monogr. Ser.*, vol. 31, edited by V. Dehant et al., pp. 251–261, AGU, Washington, D. C.

Ponte, R. M., D. Stammer, and J. Marshall (1998), Oceanic signals in observed motions of the Earth's pole of rotation, *Nature*, *391*, 476–479.

Raisanen, J. (2003), CO_2-induced changes in atmospheric angular momentum in CMIP2 expermients, *J. Clim.*, *16*, 132–143.

Rosen, R. D., and D. A. Salstein (2000), Multidecadal signals in the interannual variability of atmospheric angular momentum, *Clim. Dyn.*, *16*, 693–700.

Rowell, D. (1998), Assessing potential seasonal predictability with an ensemble of multidecadal GCM simulations, *J. Clim.*, *11*, 109–120.

Schuh, H., S. Nagel, and T. Seitz (2001), Linear drift and periodic variations observed in long time series of polar motion, *J. Geod.*, *74-10*, 701–710, DOI:10.1007/s001900000133.

Schultz, M., and M. Mudelsee (2002), REDFIT: Estimating red-noise spectra directly from unevenly spaced paleoclmatic time series, *Comput. Geosci.*, *28*, 421–426.

Torrence, C., and G. P. Compo (1998), A practical guide to wavelet analysis, *Bull. Am. Meteorol. Soc.*, *79*, 61–78.

Wilson, C. R., and R. O. Vicente (1990), Maximum likelihood estimates of polar motion parameters, *Variations in Earth Rotation*, *Geophys. Monogr. Ser.*, vol. 59, edited by D. D. McCarthy and W. E. Carter, pp. 151–155, AGU, Washington, D. C.

C. Bizouard, Observatoire de Paris/SYRTE, 61 avenue de l'Observatoire, F-75014 Paris, France. (christian.bizouard@obspm.fr)

O. de Viron, Observatoire Royal de Belgique, 3, Avenue Circulaire, B-1180 Brussels, Belgium. (o.deviron@oma.be)

L. Fernandez, CONICET/Facultad de Ciencias Astronomicas y Geofisicas, Paseo del Bosque s/n (B1900FWA) La Plata, Buenos Aires, Argentina. (lauraf@fcaglp.unlp.edu.ar)

D. A. Salstein, Atmospheric and Environmental Research, Inc., 131 Hartwell Avenue, Lexington, MA 02421-3126, USA. (salstein@aer.com)